

Changes in irreversibility line, anisotropy, and condensation energy by oxygen depletion of $\text{YBa}_2\text{Cu}_3\text{O}_{7-\delta}$

D. Babić*

*Interdisciplinary Research Centre in Superconductivity, University of Cambridge, Madingley Road,
Cambridge CB3 0HE, United Kingdom*

and Department of Physics, Faculty of Science, University of Zagreb, Bijenička 32, HR-10001 Zagreb, Croatia

J. R. Cooper†

*Interdisciplinary Research Centre in Superconductivity, University of Cambridge, Madingley Road,
Cambridge CB3 0HE, United Kingdom*

J. W. Hodby and Chen Changkang

Department of Physics, University of Oxford OXI 3PU, United Kingdom

(Received 23 October 1998)

We report results of magnetization measurements on the same $\text{YBa}_2\text{Cu}_3\text{O}_{7-\delta}$ crystal for a range of δ values $0.03 \leq \delta \leq 0.35$, in magnetic fields up to 120 kOe, applied parallel or perpendicular to the CuO_2 planes. Zero-field resistivity anisotropy measurements have also been made for the same values of δ . The irreversibility line H_{irr} falls by over a factor of 10 in the range of δ studied, and there is a similar strong decrease in superconducting condensation energy associated with the growth of the normal-state pseudogap in underdoped cuprates. On the other hand, the anisotropy in H_{irr} and the room-temperature resistivity anisotropy only increase by a factor of 2. Evidence that for our crystals the so-called ‘‘vortex lattice melting line’’ $H_m(T) \approx H_{irr}(T)$ is presented. There is also a large field and temperature region where the reversible magnetization varies as $H^{-1/2}$ and its magnitude corresponds to a free-energy density of $k_B T$ in a certain field-dependent correlation volume. Many of the results are consistent with the presence of critical thermodynamic fluctuations described by the three-dimensional XY model; these are probably enhanced when the field along the c axis is greater than 10 kOe. [S0163-1829(99)02825-8]

I. INTRODUCTION

The irreversibility line H_{irr} is a characteristic boundary in the field-temperature H - T phase diagram of high-temperature superconductors above which there is still a relatively large diamagnetic signal (of the magnitude expected from standard Ginzburg-Landau theory), but the magnetization versus field $M(H)$ curves are perfectly reversible and the resistivity is finite. This line is therefore of considerable technical importance because it determines the power dissipation in an applied magnetic field. $\text{YBa}_2\text{Cu}_3\text{O}_7$ or $\text{YBCO}(7)$ is particularly interesting because for $H \parallel c$ it has the highest irreversibility line $H_{irr}^c(T/T_c)$ of all known high- T_c superconductors. The relationship between $H_{irr}^c(T)$ and the so-called vortex lattice melting line, $H_m^c(T)$, at which there is a weakly first-order phase transition¹ is also of interest. Small-angle neutron-scattering work² shows that the flux-line lattice disappears at $H_m^c(T)$ but so far has given no evidence for a liquid of line vortices above $H_m^c(T)$. Nor is there any clear evidence from flux transformer experiments for nonlocal electrical conductivity that could be ascribed to line vortices above $H_m^c(T)$.³ As discussed further in Sec. III C, whatever its nature, it is very probable that the melting line represents an upper limit to $H_{irr}^c(T)$ and that in typical twinned $\text{YBCO}(7)$ crystals there are usually enough defects to pin the vortex lattice and give some detectable magnetic hysteresis (on the time scales used in the present work, namely, field

sweep rates of 20–200 Oe/s) as soon as the flux-line lattice is formed at $H_m^c(T)$.^{4–8}

For such crystals it was shown recently⁴ that with a magnetic field H applied parallel to the crystallographic c axis, the corresponding irreversibility line $H_{irr}^c(T)$ occurs at a fixed point on the three-dimensional (3D) XY scaled magnetization curves, indicating that at $H_{irr}^c(T)$, and by implication $H_m^c(T)$, the free energy in a coherence volume is a fixed multiple of $k_B T$ (k_B being Boltzmann’s constant). Integration of the experimental $M(H)$ curves⁴ showed this multiple to be $0.3–1 k_B T$ suggesting that thermodynamic fluctuations have a crucial influence on the melting and irreversibility lines over a substantial temperature region around T_c , much wider than that given by the reduced Ginzburg temperature t_G .^{9,10} Thus, for fully oxygenated YBCO , and for $H \parallel c$, the shape of H_{irr}^c for $t < 0.3$ is determined by the power law $H_{irr}^c = H^* t^{4/3}$, where $t = 1 - T/T_c$, and its magnitude is characterized by the prefactor H^* .

It is known¹¹ that the behavior outlined above changes with the oxygen depletion δ in $\text{YBa}_2\text{Cu}_3\text{O}_{7-\delta}$. Removal of oxygen from the conducting CuO chains increases the anisotropy in physical properties parallel and perpendicular to the c axis, and is expected to give a more pronounced 2D behavior. However, in the same range of δ , specific-heat measurements show a large decrease in the condensation energy density $H_c^2(0)/8\pi$.¹² In this paper we report experimental data that seem to distinguish between the influences of

increased anisotropy and decreased condensation energy on H_{irr}^c as δ is increased. We also discuss 3D XY scaling for $H\|c$ in a wide oxygen-doping range, showing that although $H_{irr}^c(T)$ sometimes deviates from being a fixed point on 3D XY plots, 3D XY scaling of the reversible magnetization still holds in certain areas of the H - T phase diagram.

II. EXPERIMENT

The crystals were grown from flux in an Y_2O_3 crucible (with 1% BaO as binder), using 99.999% purity chemicals.¹³ Two twinned YBCO single crystals from the same batch were annealed in flowing oxygen at selected temperatures and quenched into liquid nitrogen in order to change δ . After quenching they were held at room temperature for at least 12 h so that any short-range ordering of the oxygen atoms¹⁴ could stabilize. Their zero-field T_c values and transition widths were measured using an ac susceptometer, and checked in subsequent magnetization or resistivity measurements. The resistivity anisotropy γ_{res} of the smaller sample (Y1) was measured using the Montgomery method,¹⁵ and this is compared with the change in anisotropy obtained from the magnetization measurements. The resistivity results were checked for $\delta=0.35$ using a third crystal. The larger crystal (Y2; 5.3 mg, $1.59 \times 1.52 \times 0.34$ mm³) was used for magnetization measurements with $H\|c$ and $H\|ab$, using a vibrating sample magnetometer (VSM) and a superconducting quantum interference device (SQUID) magnetometer. The various values of δ were obtained by annealing in flowing oxygen for ~ 10 days at the following temperatures (and in the following order): 600 °C ($\delta=0.21$, $T_c=83.7$ K), 560 °C ($\delta=0.15$, $T_c=91.0$ K), 500 °C ($\delta=0.08$, $T_c=93.2$ K), 710 °C ($\delta=0.35$, $T_c=61.4$ K), 420 °C ($\delta=0.03$, $T_c=91.3$ K). The values of δ were derived from the annealing temperatures using our own unpublished data and published equilibrium oxygen-pressure curves for single-phase polycrystalline YBCO.¹⁶ The estimated uncertainty in the values of δ listed above is ± 0.02 . The T_c values were determined using a Lake Shore ac susceptometer (ACS) (samples Y1, Y2), an Oxford Instruments VSM and a Quantum Design SQUID magnetometer (sample Y2), and by resistivity measurements (sample Y1). All magnetization measurements were carried out for both $H\|c$ and $H\|ab$. We found no discrepancy between the above measurements of T_c within experimental error. The T_c values were taken as the midpoints of the 10–90% ACS transition points. The 10–90% transition widths ΔT_c were found to *increase with increasing* δ , and ranged from 0.4 K ($\delta=0.03$) to 1.8 K ($\delta=0.35$). Repeated annealing and quenching did not reduce these transition widths. The increase in ΔT_c with δ could possibly arise from short-range ordering or clustering of the oxygen atoms at room temperature,¹⁴ or from increased 2D character. In support of the latter point we note that ΔT_c of highly anisotropic $Bi_2Sr_2CaCu_2O_{8+x}$ (Bi2212) is invariably at least 2 K.

The electrical contacts on the sample Y1 were made using 25- μ m-diam gold wires and DuPont 6838 silver paste, fired at 420 °C in flowing oxygen for 5 min. This procedure gave contact resistances of a few ohms per contact. After the resistivity measurements had been completed for a given δ , the silver contacts were removed by etching the sample in a

solution of 4% Br in ethanol for 20 min, followed by further cleaning in an ultrasonic bath. Each etch reduced the sample dimensions by less than 1 μ m per side. The resistivity measurements were carried out using a low-frequency ac method, with the contacts in a Montgomery geometry, i.e., with two line contacts on each ab face of the crystal platelet. The size of the crystal was $1 \times 0.8 \times 0.09$ mm³ with the short dimension corresponding to the c direction and the distance between the contacts was 0.8 ± 0.1 mm.

The VSM measurements on sample Y2 were carried out using both field sweeps and zero-field-cooled (ZFC) and field-cooled (FC) temperature sweeps. The field-sweep rate was 20–200 Oe/s, and for these speeds we found no dependence of H_{irr} on the sweep rate. The temperature-sweep rates were 0.011 K/s for ZFC and FC, and 0.003 K/s for the measurements of T_c in 5 Oe. In many cases there were clear changes in slope of the FC and ZFC $M(T)$ curves in the reversible region and these could be used to define $H_m(T)$. The values of H_{irr} determined from the point at which there was a significant difference between ZFC and FC $M(T)$ curves were typically 30% less than those from the $M(H)$ loops and showed a somewhat stronger T dependence. As before,⁴ these differences are ascribed to flux creep during the slower temperature sweeps. In our further discussions we use H_{irr} determined from the field sweeps but the relationship between H_{irr} and $H_m(T)$ is considered again in Sec. III C. The superconducting contribution to the total magnetization was extracted by subtracting the normal-state paramagnetism of the sample measured above T_c using a more sensitive SQUID magnetometer. Corrections were made for the changes in the intrinsic spin susceptibility in the superconducting state given by electron spin resonance studies¹⁷ and the effect of the normal-state gap derived from NMR work.¹⁸ Typical uncertainties in these corrections are $\pm 15\%$ of the spin susceptibility of YBCO(7) giving $\pm 4 \times 10^{-5}$ emu (0.05 G) at 120 kOe or $\pm 1.8 \times 10^{-6}$ G K⁻¹ Oe^{-1/2} on the 3D XY scaled plots shown below in Fig. 6. For $T_c=61.4$ K, corrections for a small Curie term (0.01 emu K/mol) arising from paramagnetic impurities or defects have also been made. In Fig. 6 below, they are significant at the level of $\pm 3.6 \times 10^{-6}$ G K⁻¹ Oe^{-1/2}.

III. MAGNETIZATION MEASUREMENTS

A. Raw magnetization data

In Fig. 1 we show typical results of the magnetization-loop measurements for $H\|c$ [expressed as the measured magnetic moment m (emu)] after subtracting the normal-state paramagnetic contribution. The δ values increase from 0.03 to 0.35, as indicated, while the T/T_c values are chosen to be 0.83–0.84. It is clear that the irreversibility points are clearly defined. At high fields the reversible magnetization falls approximately as the condensation energy (shown later in Fig. 10) but its value just above $H_{irr}(T)$ is always in the range -0.001 to -0.0015 emu or -1.2 to -1.8 G at the reduced temperatures shown.

B. Irreversibility lines for $H\|c$

In the experimentally accessible region of its H - T diagram ($0.01 \leq t \leq 0.2$ and $3 \text{ kOe} \leq H \leq 120 \text{ kOe}$), H_{irr}^c of

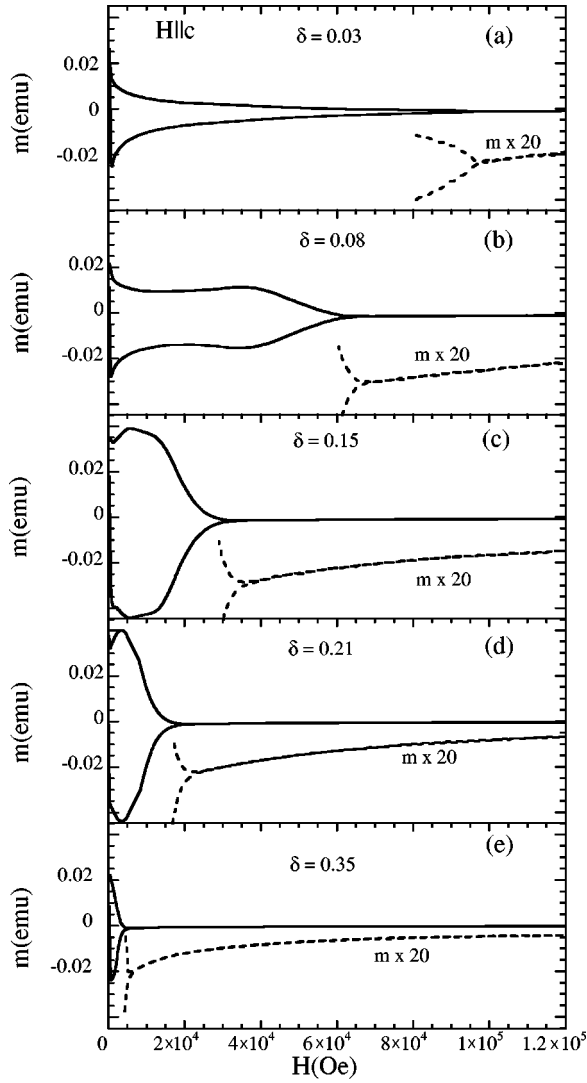


FIG. 1. Measured magnetic moment ($m = MV$) loops for $H\parallel c$ after subtraction of the normal-state paramagnetic signal. The δ values increase from 0.03 (a) to 0.35 (e), and $T/T_c \sim 0.83 - 0.84$ for all the data shown.

YBCO(7) exhibits a $t^{4/3}$ temperature dependence.⁴ More anisotropic high- T_c compounds have lower $H_{irr}^c(t)$, and at low temperatures tend to show deviations from power-law behavior.^{19,20} More precisely, an initial power law $H_{irr}^c \propto t^n$, where $n = 1 - 1.5$, changes at low temperatures to a straight line on a $\ln H_{irr}^c$ versus T plot. For both highly anisotropic Bi2223 and Bi2212, $H_{irr}^c = H_0 \exp(-T/T_0)$ is observed at low temperatures and over a wide range of T .^{20,21} A similar increase in H_{irr}^c above an initial power-law dependence was found for oxygen-deficient YBCO as well,¹⁹ indicating a similar exponential form of H_{irr}^c at low temperatures. In general, the lower values of H_{irr}^c for the more anisotropic high- T_c systems allow larger and different regions of the $H_{irr}^c(T)$ line to be investigated. As an illustration of this, in Fig. 2 we show H_{irr}^c for the two limiting cases of our work, $\delta = 0.03$ (a) and $\delta = 0.35$ (b). The solid lines are fits to the power law (a) and the exponential law (b). As mentioned before, the law $H_{irr}^c \propto t^{4/3}$ has a natural description within the framework of 3D XY fluctuation theory, while the exponential dependence has often been observed in Josephson-coupled layered high-

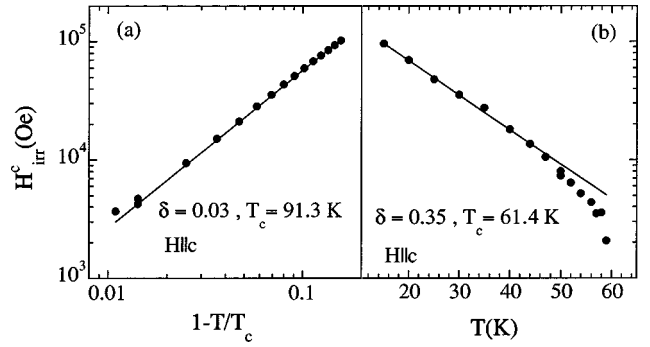


FIG. 2. Irreversibility lines H_{irr}^c for $H\parallel c$ for the two limiting values of δ . (a) H_{irr}^c for $\delta = 0.03$, showing $(1 - T/T_c)^{4/3}$ dependence (straight line). (b) H_{irr}^c for $\delta = 0.35$, showing $\exp(-T/T_0)$ dependence (straight line) for $T/T_c \leq 0.77$.

T_c superconductors such as Bi2212. Here we simply use the plot in Fig. 2(b) as an appropriate and simple description of the change of the shape of H_{irr}^c , its underlying cause is discussed in Refs. 19 and 20.

Figure 3 shows H_{irr}^c versus t for all values of δ studied. For $0.15 \geq \delta \geq 0.03$ there is a reasonably large region that can be fitted by a $t^{4/3}$ power law. For $\delta = 0.21$ and $\delta = 0.35$ the data give a better fit to $n = 1$ rather than $n = 4/3$ between $t = 0.01$ and $t = 0.1$ (even after taking into account the increased zero-field transition widths and the associated error in T_c). It possibly arises because the critical behavior giving $n = 4/3$ is induced by the application of a field greater than 10 kOe along the c axis. For increasing δ there is some evidence for a change in the functional form (shape) of $H_{irr}^c(t)$. Namely, for $\delta = 0.35$ the $n = 1$ power law mentioned above may go over directly to an exponential law at higher values of t [Fig. 2(b)]. However we have estimated the magnitude of $H_{irr}^c(T/T_c)$ by fitting all curves to a $4/3$ power law, as shown by the solid lines in Fig. 3, i.e., by determining the parameter H^* in the law $H_{irr}^c = H^* t^{4/3}$. Clearly, this is only approximate for $\delta = 0.21$ and $\delta = 0.35$. However fits to the

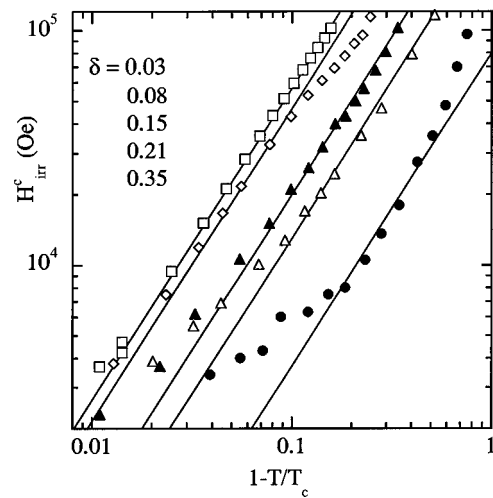


FIG. 3. Irreversibility lines H_{irr}^c vs $(1 - T/T_c)$ on a log-log plot, for all δ values investigated. The straight lines $H^*(1 - T/T_c)^{4/3}$ are drawn through regions where there is satisfactory 3D XY scaling of the reversible magnetization. The values of H^* decrease monotonically from 1225 kOe to 80 kOe as δ increases from 0.03 to 0.35.

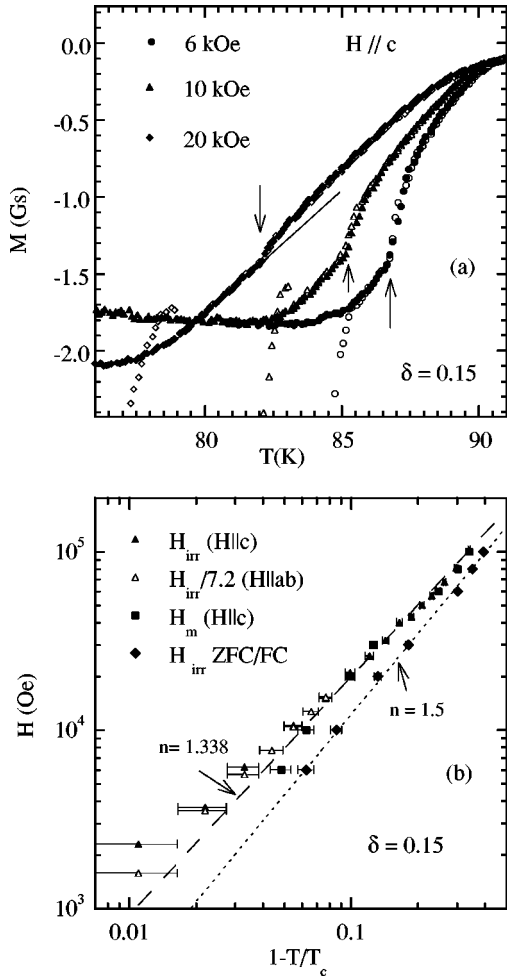


FIG. 4. (a) Examples of “melting” anomalies in the reversible magnetization $M(T)$ for $H \parallel c$ and $\delta=0.15$. Open symbols, ZFC data (warming); closed symbols, FC data (cooling). (b) Comparison of $H_{irr}^c(T)$, $H_{irr}^{ab}(T)$ for $\delta=0.15$ [both derived from VSM $M(H)$ loops at 20–200 Oe/s] with melting anomalies such as those (a). $H_{irr}^c(T)$ data from ZFC and FC $M(T)$ curves are also shown. They fit the $n=1.5$ power law while the other data all fit $n=4/3$.

law $H_{irr}^c = H_0 \exp(-T/T_0)$ give T_c/T_0 values of 3.3 and 4.1 and H_0 values of 570 and 279 kOe, respectively, which are only a factor of 2 or 3 larger than the corresponding values of H^* (280 and 80 kOe, respectively). Thus the overall conclusion that H_{irr}^c falls strongly with δ is valid both in the power-law region near T_c and the exponential region well below T_c .

C. Relationship between $H_{irr}^c(T)$ and the melting line $H_m^c(T)$

For the measurements with $\delta=0.15$ and $H \parallel c$ there are well-defined anomalies in the reversible regions of the ZFC and FC $M(T)$ plots, some of which are shown in Fig. 4(a). These are thought to mark the melting line $H_m^c(T)$ and, as shown in Fig. 4(b), they agree extremely well with the values of $H_{irr}^c(T)$ determined from closure of the $M(H)$ loops taken with the VSM and also obey a 4/3 power law. However, the values of $H_{irr}^c(T)$ obtained from closure of the FC and ZFC $M(T)$ curves are 20–40 % lower and fit an $n=1.5$ power law better than $n=4/3$. We attribute these differences to the

effects of flux creep during the slower ZFC and FC temperature sweeps. Namely, the flux-line lattice is formed at $H_m^c(T)$, but because of flux creep on long time scales $H_{irr}^c(T)$ is significantly smaller than $H_m^c(T)$ when the temperature is swept slowly in fixed fields. There is also some evidence for melting anomalies at $\delta=0.21$ from changes in slope of $M(T)$ but they are not as sharp. It seems that $\delta=0.15$ (corresponding to an annealing temperature of 560 °C) is particularly favorable for observing melting because the twin structure is less well developed but the condensation energy is still large enough to give a clear anomaly. The FC and ZFC data for $\delta=0.15$ (and for 0.21—not shown here) provide direct evidence that $H_{irr}^c(T)$ obtained from VSM $M(H)$ sweeps at 200-Oe/s is almost identical to $H_m^c(T)$. However for $\delta=0.35$, where any changes in slope in $M(T)$ are only just visible, $H_{irr}^c(T)$ from the 200 Oe/s VSM field sweeps seems to be a factor of 2 less than $H_m^c(T)$, probably because of even weaker pinning of the flux-line lattice associated with the extremely low condensation energy.

The relationship between H_m and H_{irr} has been discussed recently by Willemin *et al.*²² who also found that the measurement procedure has an important effect. By applying a small additional ac field H_{ac} in their magnetic-torque measurements they have shown that H_{irr} is essentially equal to H_m at $H_{ac}=0$ and drops well below H_m when $H_{ac} \neq 0$. The effects of their ac field and our slow ZFC/FC T sweeps on H_{irr} have the same physical origin. In their case, vortex creep is enhanced by shaking the vortices out of their pinning sites with an ac field, whereas in our case there is significant creep when a fixed field is applied for a long time. They also find that $H_{irr} \approx H_m$ when the vortex creep is suppressed and that $H_{irr} < H_m$ when it is not, as well as the 4/3 power law when $H_m \approx H_{irr}$. These two independent and complementary approaches both lead to the conclusion that H_m and H_{irr} are the same in YBCO *only* if there is negligible vortex creep on a time scale of the measurement. For very low condensation energies it is probable that only quite rapid measurements would give $H_m \approx H_{irr}$.

D. Anisotropy in the irreversibility lines

For $H \parallel c$ the appropriate coherence length is ξ_{ab} , while for $H \parallel ab$ the coherence scale is $(\xi_{ab}\xi_c)^{1/2} < \xi_{ab}$. This means that in an anisotropic 3D picture characteristic properties for $H \parallel c$ and $H \parallel ab$, such as lines in the H - T diagram, should scale with the anisotropy parameter $\gamma = \xi_{ab}^0/\xi_c^0$ and are expected to be higher for $H \parallel ab$ than for $H \parallel c$. In the case of H_{irr}^c ($\delta=0.03$), with well-defined $t^{4/3}$ behavior, in the critical region we expect $H_{irr}^c \propto \xi_{ab}^{-2}$. As discussed in Sec. III E, 3D XY scaling for $H \parallel ab$ introduces the scaling variable of the free-energy density as $z = H \xi_{ab} \xi_c / \Phi_0$, and the ratio $\gamma_{irr} = H_{irr}^{ab}/H_{irr}^c$ is only expected to be exactly equal to the anisotropy parameter γ if both H_{irr}^c and H_{irr}^{ab} occur at fixed points of the 3D XY magnetization plots. However, if the reversible-magnetization data collapse on to a 3D XY curve of a reasonably small width and if the broadening of H_{irr} around a fixed point is reasonably small for the both field orientations, then γ_{irr} should still be a good estimate of γ .

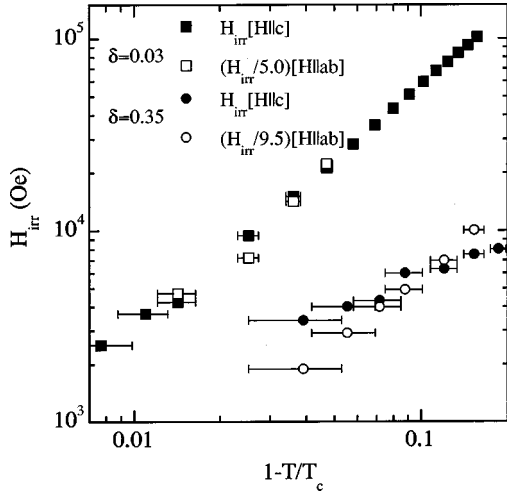


FIG. 5. Irreversibility lines H_{irr}^c ($H||c$) and $H_{irr}^{ab}/\gamma_{irr}$ ($H||ab$) for the two limiting values of δ . The other irreversibility lines are intermediate between the two extremes shown, with γ_{irr} changing monotonically from 5.0 to 9.5 as δ increases from 0.03 to 0.35.

In Fig. 5 we show H_{irr}^c and $H_{irr}^{ab}/\gamma_{irr}$ for $\delta=0.03$ and $\delta=0.35$ plotted against t on a log-log plot. The data for the other oxygen concentrations lie in between these two extremes. Since H_{irr}^c and H_{irr}^{ab} do not have exactly the same t dependence, there is an uncertainty of at least ± 0.3 for each $\gamma_{irr}(\delta)$. This analysis shows that γ_{irr} increases smoothly from 5 ($\delta=0.03$) to 9.5 ($\delta=0.35$) as δ increases, that is by approximately a factor 2, while H^* decreases by more than a factor of 10 [1225 kOe ($\delta=0.03$) to 80 kOe ($\delta=0.35$)].

E. 3D XY scaling

The free-energy density f_s of a superconductor in a magnetic field in the presence of thermodynamic fluctuations can be written as^{23,24}

$$f_s = f_n - \frac{Ck_B T}{V_c} G \left(\frac{H\xi^2}{\Phi_0} \right), \quad (1)$$

where f_n is the normal-state free-energy density, C a constant of order unity, $V_c = \xi_{ab}^2 \xi_c$ a T -dependent correlation volume, ξ a coherence scale, and G an unknown scaling function. For $H||c$, $\xi = \xi_{ab}$, and for $H||ab$, $\xi = (\xi_{ab} \xi_c)^{1/2}$. Taking the first derivatives with respect to H gives the fluctuation magnetizations $M_{ab,c}$ (where subscripts denote directions of the applied magnetic field):

$$\frac{M_{ab,c}}{H^{1/2}} = - \frac{Ck_B T}{\Phi_0^{3/2}} \Gamma_{ab,c}, \quad (2)$$

where $\Gamma_c = \gamma G'(y)/y^{1/2}$, $\Gamma_{ab} = \gamma^{-1/2} G'(y/\gamma)/(y/\gamma)^{1/2}$. For the 3D XY universality class $y = H(\xi_{ab}^0)^2/\Phi_0 t^{2\nu}$, and $\nu = 2/3$ is the appropriate critical exponent for the temperature dependence of the coherence lengths. Thus, theoretically speaking, in the critical region it is possible to observe scaled $M/TH^{1/2}$ versus $H/t^{4/3}$ curves not only for $H||c$ but also for $H||ab$. The results for $H||c$ can be discussed with more certainty, because the stiffness of the system for $H||ab$ means that the reversible region occurs over a much smaller tem-

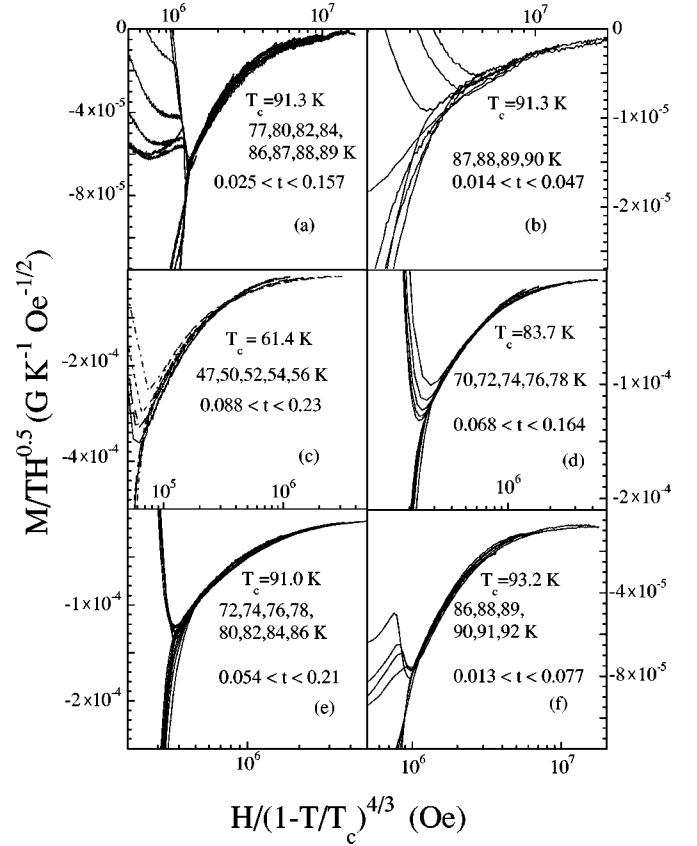


FIG. 6. 3D XY scaling of the measured magnetization ($M = m/V$). (a) $\delta=0.03$, $H||c$. This result was known previously (Ref. 4). (b) $\delta=0.03$, $H||ab$. The characteristic structure of 3D XY scaling is clearly visible, although the range of analysis is restricted to a narrow region in the H - T plane. (c)–(f) $0.08 \leq \delta \leq 0.35$ and $H||c$. The δ values are (c) 0.35, (d) 0.21, (e) 0.15, (f) 0.08. The temperature ranges where 3D XY plots show satisfactory quality are indicated.

perature range and also the corrections for the normal-state spin susceptibility and paramagnetic impurities are more significant.

In Figs. 6(a) and 6(b) we show the 3D XY scaled magnetization curves for $\delta=0.03$ for both $H||c$ (a) and $H||ab$ (b). The results in Fig. 6(a) were shown previously,⁴ and we plot them again for completeness. We note the characteristic structure of 3D XY scaling shown in Fig. 6(b), for $H||ab$, which justifies the prediction of Eq. (2).

In Figs. 6(c)–6(f) we show the 3D XY scaled magnetization curves for the other δ values, with $H||c$. Taking into account the uncertainties in the normal-state paramagnetism mentioned in Sec. II, there is good 3D XY scaling of the reversible magnetization for all curves in the region $0.07 < t < 0.15$ – 0.2 . However as δ is increased the scaling breaks down at certain values of t (0.05 for $\delta=0.15$ and 0.07 for $\delta=0.35$). As discussed in connection with $H_{irr}(t)$ in Sec. III B, this probably represents different physics (an exponent $n=1$). It is interesting to note that a relatively broad 3D XY scaling region has been observed²⁵ for extremely 2D Bi2212 crystals for $H||c$ in the range $0.04 < t < 0.24$, but with a different scaling function.

To conclude this subsection, the results we presented show that for YBCO ($7-\delta$) thermodynamic fluctuations of

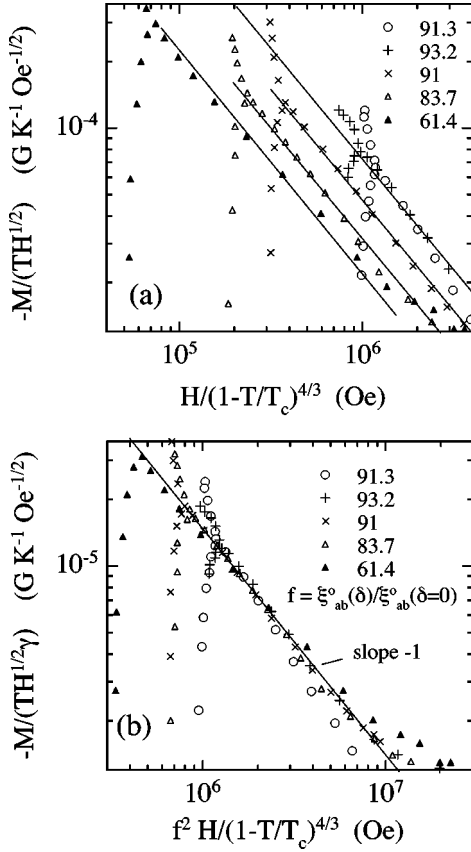


FIG. 7. (a) Log-log plots of the 3D XY scaled magnetization ($M = m/V$) curves shown in Fig. 6 for $H\parallel c$. Note the extended regions of slope -1 , showing that over much of the reversible region the scaled magnetization is proportional to $1/y$, where y is the 3D XY scaling variable $H\xi_{ab}^2$. (b) Scaled 3D XY plots according to Eq. (4). The vertical scaling factor is the measured anisotropy γ_{irr} and the horizontal one is $(\xi_{ab}^0)^2$. Both parameter values are given in Table I. The H_{irr}^c values scale adequately except for $\delta = 0.35$ probably because for this value of δ , H_{irr}^c is a factor of 2 lower than H_m^c , as mentioned in Sec. III C.

the 3D XY class play an important role above and around H_{irr} , for both $H\parallel c$ and $H\parallel ab$.

F. Form of 3D XY scaling plots

It is informative to look at the form of the various 3D XY plots for $H\parallel c$ shown in Fig. 6 in more detail. This has been done by making the log-log plots shown in Fig. 7. Surprisingly, all these curves show a $1/y$ behavior that in several cases extends over more than one decade in y . In terms of

Eq. (2) this implies that $G'(y) \propto y^{-1/2}$ and that the dominant field-dependent contribution to $G(y)$ is $\propto y^{1/2}$. From Eq. (1) this gives

$$f_s = f_n - F(T) + \frac{Ck_B T \gamma}{\xi_{ab}^2} \sqrt{\frac{H}{\Phi_0}}, \quad (3)$$

where $F(T)$ is essentially field independent. If the constant $C \approx 1$, then the field-dependent contribution to the free-energy density in Eq. (3) is equal to $k_B T$ in the characteristic volume $\xi_{ab} \xi_c \sqrt{\Phi_0/H}$. The corresponding form of the magnetization is

$$M_c = -\frac{Ck_B T \gamma}{2\xi_{ab}^2} \sqrt{\frac{1}{\Phi_0 H}}. \quad (4)$$

Taking the constant C to be slightly more than unity (1.5), $\xi_{ab}^0 = 12.6 \text{ \AA}$ [corresponding to a coherence volume $(\xi_{ab}^0)^3/\gamma$ of $400 (\text{\AA})^3$ for YBCO(7) [Ref. 4] together with the measured value of $\gamma_{irr} = 5$, leads to values of $M(T, H)$, which are in remarkable agreement with the experimental data (to within a few percent) between H_{irr}^c and $2H_{irr}^c$. For higher values of δ , the field range where there is $1/y$ behavior is much wider as shown in Fig. 7, and in order to account for the magnitude of $M(H, T)$ in terms of Eq. (4) (using the measured values of γ_{irr}) the ab -plane coherence length ξ_{ab}^0 must increase with δ by a factor of 2.5 from $\delta = 0$ to $\delta = 0.35$ as shown later in Table I. Preliminary measurements of the fluctuation magnetization above T_c for the same crystal provide support for this scenario in that the results are consistent with such changes in ξ_{ab}^0 with δ . Furthermore, as also shown in Table I, these values of ξ_{ab}^0 are consistent with the product $H_c^2(0)(\xi_{ab}^0)^3/8\pi\gamma T_c$ being approximately constant as expected for critical fluctuations described by the 3D XY model.⁴ This product is in fact the condensation energy in a coherence volume at $T = 0$ measured in units of T_c . It is surprisingly small, ranging from 0.15 – $0.23k_B$. In summary, the form of Eq. (4) should provide an important clue towards understanding the so-called ‘‘vortex liquid’’ phase.

G. Resistivity anisotropy

Resistivity measurements provide information about the anisotropy independently of magnetization measurements. The most widely used expression for the anisotropy parameter is the square root of the resistivity ratio, i.e., $\gamma_{res} = (\rho_c/\rho_{ab})^{1/2}$ [the subscripts denote the resistivities perpendicular (c) and parallel to the planes (ab)]. In the anisotropic

TABLE I. Summary of various parameters measured or derived in the present work. All symbols are defined in the text except for K , which is equal to $H_c^2(0)(\xi_{ab}^0)^3/8\pi\gamma_{irr}T_c$ and is expected to be constant in a 3D XY critical fluctuation picture.

δ	T_c (K)	$H_c^2(0)$ (kOe ²)	H^* (kOe)	γ_{irr}	γ_{res}	$\xi_{ab}^0(\delta)/\xi_{ab}^0(\delta=0)$	$K(k_B)$
0.03 ± 0.02	91.3	120	1225	5.0	4.96	1	0.15
0.08	93.2	110	1000	6.5	4.76	1.14	0.16
0.15	91.0	83 ± 6	430	7.2	5.40	1.45	0.23
0.21	83.7	38 ± 7	280	8.0	6.70	1.90	0.22
0.35	61.4	14	80	9.5	8.05	2.45	0.20

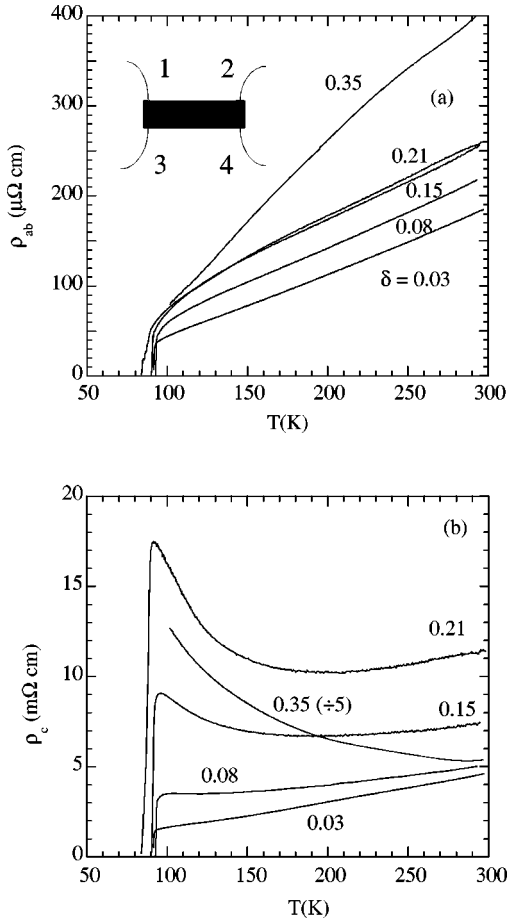


FIG. 8. Resistivities ρ_{ab} (a) and ρ_c (b) determined by the Montgomery method. For $\delta=0.35$ the Montgomery resistance R_{12} could not be detected below ~ 100 K and lower-temperature data are missing. The geometry used for the Montgomery method is shown in the inset to (a).

effective mass or the anisotropic Ginzburg-Landau (GL) model, the anisotropy in the superconducting state, i.e., the ratio of the coherence lengths ξ_{ab} and ξ_c , equals γ_{res} defined above. In the case of untwinned YBCO crystals, the resistivity ρ_b along the conducting CuO chains is lower than the resistivity ρ_a perpendicular to the chains, which introduces a threefold anisotropy.²⁶ However our samples are twinned, and the measured ρ_{ab} is an average of ρ_a and ρ_b , including some contribution of the twin boundaries as well.²⁶ An appropriate method for measuring both ρ_c and ρ_{ab} is the Montgomery method¹⁵ that is based on measuring the resistances $R_{ij}=V_{ij}/I_{kl}$, where i,j and k,l are four electrical contacts. Two of them (1,2) are made to the top surface of the crystal platelet, and the other two (3,4) to the bottom, with the c axis perpendicular to the surface as sketched in the inset to Fig. 8(a). We applied this method to the sample Y1, using a low-frequency ac current of $100 \mu\text{A}$. A consistency check was made using a second crystal with $\delta=0.35$, for which the results obtained agreed to within 10–15 %.

In Fig. 8(a) we show our results for ρ_{ab} and in Fig. 8(b) for ρ_c . The results are in rather good agreement with published work^{26–29} although checks should be made for other crystals before discussing details such as the precise T dependences of ρ_{ab} and ρ_c . The data for $\delta=0.35$ are missing

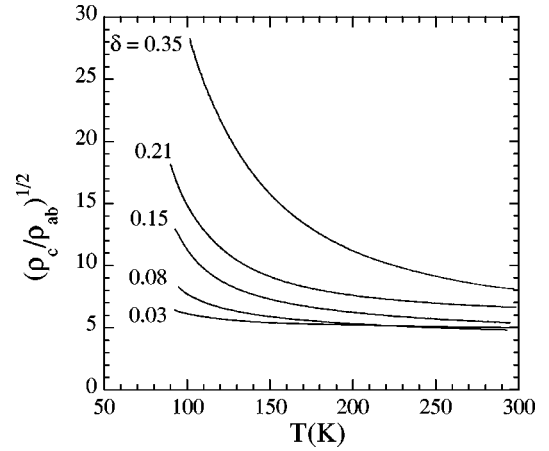


FIG. 9. Anisotropies $\gamma_{res} \equiv (\rho_c/\rho_{ab})^{1/2}$ found from the resistivity curves in Fig. 8.

at low temperatures because at this relatively high level of anisotropy, R_{12} was too small to be measured below ~ 100 K.

For the purpose of our present work the most interesting quantity is the change in anisotropy with δ . We define the resistivity anisotropy $\gamma_{res} = (\rho_c/\rho_{ab})^{1/2}$ in the usual way, and the results are shown in Fig. 9. It is clear that γ_{res} is temperature dependent and that it increases with decreasing temperature. The temperature dependence becomes weaker with decreasing δ , ending finally in an almost temperature-independent curve for $\delta=0.03$. We assign this behavior to the presence of the normal-state gap in oxygen-deficient samples,³⁰ which probably has a stronger effect on ρ_c than ρ_{ab} and is therefore responsible for the temperature dependence of γ_{res} . The marked temperature dependence of γ_{res} raises the question as to how it can be used to estimate the anisotropy. Because of the existence of the normal-state gap, we believe that the high-temperature values of γ_{res} give the best measure of the band-structure anisotropy. Indeed, at room temperature all the anisotropy curves are reasonably flat with respect to temperature, including that for $\delta=0.35$. We note that the change in γ_{res} (290 K) is moderate, and that it ranges from 4.96 ($\delta=0.03$) to 8.05 ($\delta=0.35$). It is interesting to note that it is the room-temperature resistivity anisotropy γ_{res} (290 K), rather than γ_{res} just above T_c that agrees with the anisotropy in H_{irr} (Sec. III D).

IV. IRREVERSIBILITY LINES, ANISOTROPY, AND CONDENSATION ENERGY

In this section we summarize results presented previously and establish connections between H_{irr}^c , the anisotropy, and the condensation energy. The specific-heat data from Ref. 12 give the δ dependence of the condensation energy density $H_c^2(0)/8\pi$. Up to this point we have shown that the anisotropies γ_{irr} and γ_{res} , in the irreversibility field and room-temperature resistivity respectively, increase approximately by a factor of 2, while H_{irr} decreases by more than a factor of 10 when δ increases from 0.03 to 0.35. We summarize these results in Table I and also in Fig. 10 where we plot several important quantities as functions of δ : $H_c^2(0)$, H^* [Fig. 10(a)], and T_c , γ_{irr} , and γ_{res} [Fig. 10(b)]. The com-

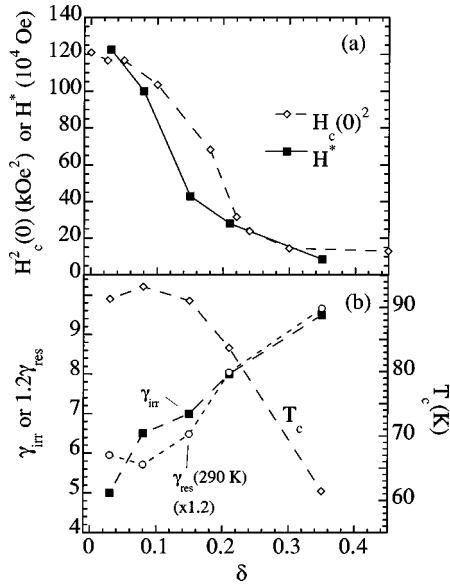


FIG. 10. (a) H^* , $H_c^2(0)$, and (b) the anisotropies γ_{irr} , γ_{res} (left-hand scale) and T_c (right-hand scale) plotted versus δ . The condensation energy is obtained by integrating specific-heat data from Ref. 12, while the other quantities are the results of the present work. Note the similarity between the condensation energy and the magnitude of the irreversibility line H^* , as well as the agreement between the two measures of anisotropies (with a scaling factor of 1.2).

parison of $H_c^2(0)$ and H^* reveals a striking similarity between these two quantities, showing the close mutual relation between the ‘‘strength’’ of superconductivity [$H_c^2(0)$] and the irreversibility line H^* , which is also a measure of the resistance of the vortex solid to melting (see Sec. III C for details). It is not the maximum T_c that determines the thermodynamic stability of the vortex solid, but the product of the pair density and the energy per superconducting pair, i.e., the condensation energy. Thus, although the change in anisotropy undoubtedly has some effect, we conclude that *the condensation energy predominantly determines the magnitude of the irreversibility line of YBCO(7- δ) over a significant range of δ* . If we look at the oxygen-doping dependence of the anisotropy, we see that it depends much less on δ than either $H_c^2(0)$ or H^* . Furthermore, it can be seen in Fig. 10(b) that γ_{irr} and γ_{res} have the same δ dependences. If we multiply γ_{res} with a factor of ~ 1.2 , then both anisotropies lie on the same curve.

V. SUMMARY AND CONCLUSIONS

There is experimental evidence that the strong decreases in both the irreversibility line $H_{irr}(T)$ and the melting line $H_m(T)$ with oxygen depletion are connected with the strong reduction in condensation energy associated with the presence of the normal-state pseudogap.³⁰ The changes in the anisotropy derived from the ratio of H_{irr}^{ab}/H_{irr}^c or the room-temperature resistivity are much smaller and this is supported by a previous magnetoresistance study of oxygen-depleted YBCO films that gave similar values for H_{irr}^{ab}/H_{irr}^c .²⁹ Our finding that there is an extended field region in which the reversible magnetization falls as $H^{-1/2}$ and has a magnitude corresponding to a free-energy density of $k_B T$ in the coherence volume $\xi_{ab}\xi_c\sqrt{\Phi_0}/H$ may help towards understanding the ‘‘vortex liquid’’ phase. Although there is evidence that many features of the experimental data are consistent with a 3D XY scaling picture involving critical thermodynamic fluctuations we do not have any microscopic picture for the nature of the ‘‘vortex liquid’’ phase. Other scenarios in which $H_{irr}(T)$ and $H_m(T)$ are directly linked to the out-of-plane penetration depth $\lambda_c(0)$ or to the c -axis resistivity (which is the important parameter in a Josephson-coupling model¹⁹) might also account for the strong decrease in H_{irr}^c with δ shown in Fig. 10(a). Namely, both direct measurements³¹ and optical conductivity studies³² show that $\lambda_c^2(0)$ increases by a factor of 30 from $\delta=0.03$ to 0.35. In such models the normal-state pseudogap is still important because of its effect on c axis transport. However, it is not clear whether such models can account for the variation of H_{irr}^{ab} with δ or the various 3D XY scaling properties reported here.

ACKNOWLEDGMENTS

We are grateful to A. M. Campbell, R. A. Doyle, A. Janossy, W. Y. Liang, J. W. Loram, J. E. McCrone, and J. L. Tallon for useful discussions. This work was funded by the Engineering and Physical Sciences Research Council (U.K.) Grants Nos. K33187 (Cambridge) and L28807 (Oxford). One of the authors (D.B.) received financial support from the Royal Society (U.K.), Project No. 119203 of the Ministry of Science of Croatia, and the Croatia-U.S. Joint Project No. NIST JF-136.

*Present address: Institut für Physik, Universität Basel, Klingelbergstrasse 82, CH-4056 Basel, Switzerland.

†On leave from the Institute of Physics, Zagreb, Croatia.

¹A. Schilling, R. A. Fisher, N. E. Phillips, U. Welp, W. K. Kwok, and G. W. Crabtree, Phys. Rev. Lett. **78**, 4833 (1998).

²C. M. Aegerter, S. T. Johnson, W. J. Nuttall, S. H. Lloyd, M. T. Wylie, M. P. Nutley, E. M. Forgan, R. Cubitt, S. L. Lee, D. M. Paul, M. Yethiraj, and H. A. Mook, Phys. Rev. B **57**, 14 511 (1998).

³R. A. Doyle and A. M. Campbell, Phys. Rev. Lett. **79**, 5300 (1997), and references therein.

⁴J. R. Cooper, J. W. Loram, J. D. Johnson, J. W. Hodby, and Chen

Changkang, Phys. Rev. Lett. **79**, 1730 (1997).

⁵T. Naito, T. Nishizaki, Y. Watambe, and N. Kobayashi, in *Proceedings of the 9th International Symposium on Superconductivity*, edited by S. Nakajima and M. Murakami (Springer-Verlag, Tokyo, 1997).

⁶U. Welp, J. A. Fendrich, W. K. Kwok, G. W. Crabtree, and B. W. Veal, Phys. Rev. Lett. **76**, 4809 (1996).

⁷D. E. Farrell, in *Physical Properties of High Temperature Superconductors IV*, edited by D. M. Ginsberg (World Scientific, Singapore, 1994).

⁸B. Billon, M. Charalambous, J. Chausy, P. Lejoy, R. H. Koch, and W. N. Hardy, Czech. J. Phys. **46**, 1581 (1996).

- ⁹R. Ikeda, T. Ohmi, and T. Tsuneto, *J. Phys. Soc. Jpn.* **58**, 1377 (1989).
- ¹⁰J. W. Loram, J. R. Cooper, J. M. Wheatley, K. A. Mirza, and R. S. Liu, *Philos. Mag. B* **65**, 1405 (1992).
- ¹¹M. A. Hubbard, M. B. Salamon, and B. W. Veal, *Physica C* **259**, 3098 (1996).
- ¹²J. W. Loram, K. A. Mirza, J. R. Cooper, and W. Y. Liang, *Phys. Rev. Lett.* **71**, 1740 (1993).
- ¹³Cheng Changkang, H. Yongle, J. W. Hodby, B. M. Wanklyn, A. V. Narlikar, and S. B. Samanta, *J. Mater. Sci. Lett.* **15**, 886 (1996).
- ¹⁴J. D. Jorgensen, Shiyong Pei, P. Lightfoot, Hao Shi, A. P. Paulikas, and B. W. Veal, *Physica C* **167**, 571 (1990).
- ¹⁵H. C. Montgomery, *J. Appl. Phys.* **42**, 2971 (1971).
- ¹⁶K. Conder, J. Karpinski, E. Kaldis, S. Rusiecki, and E. Jilek, *Physica C* **196**, 164 (1992).
- ¹⁷A. Jánossy, L.-C. Brunel, and J. R. Cooper, *Phys. Rev. B* **54**, 10 186 (1996).
- ¹⁸H. Alloul, T. Ohno, and P. Mendels, *Phys. Rev. Lett.* **63**, 1700 (1989).
- ¹⁹K. E. Gray, D. H. Kim, B. W. Veal, G. T. Seidler, T. F. Rosenbaum, and D. E. Farrell, *Phys. Rev. B* **45**, 10 071 (1992).
- ²⁰P. de Rango, B. Giordanengo, R. Tournier, A. Sulpice, J. Chaussy, G. Deutscher, J. L. Genicon, P. Lejay, R. Retoux, and B. Raveau, *J. Phys. (Paris)* **50**, 2857 (1989).
- ²¹E. Zeldov, D. Majer, M. Konczykowski, V. B. Geshkenbein, N. Chikumoto, and H. Shtrikman, *Europhys. Lett.* **30**, 367 (1995); D. Babić, Ph.D. thesis, University of Zagreb, 1996.
- ²²M. Willemin, C. Rossel, J. Hofer, H. Keller, A. Erb, and E. Walker, *Phys. Rev. B* **58**, R5940 (1998); M. Willemin, A. Schilling, H. Keller, C. Rossel, J. Hofer, U. Welp, W. K. Kwok, R. J. Olsson, and G. W. Crabtree, *Phys. Rev. Lett.* **81**, 4236 (1998).
- ²³D. S. Fisher, M. P. A. Fisher, and D. A. Huse, *Phys. Rev. B* **43**, 130 (1991).
- ²⁴T. Schneider, J. Hofer, M. Willemin, J. M. Singer, and H. Keller, *Eur. Phys. J. B* **3**, 413 (1998).
- ²⁵J. R. Cooper *et al.* (unpublished).
- ²⁶T. A. Friedmann, M. W. Rabin, J. Giapintzakis, J. P. Rice, and D. M. Ginsberg, *Phys. Rev. B* **42**, 6217 (1990).
- ²⁷L. Forró, C. Ayache, J. Y. Henry, and J. Rossat-Mignod, *Phys. Scr.* **41**, 365 (1990).
- ²⁸K. Takenaka, K. Mizuhashi, H. Takagi, and S. Uchida, *Phys. Rev. B* **50**, 6534 (1994).
- ²⁹A. Carrington, D. J. C. Walker, A. P. Mackenzie, and J. R. Cooper, *Phys. Rev. B* **48**, 13 051 (1993).
- ³⁰J. W. Loram, K. A. Mirza, J. R. Cooper, W. Y. Liang, and J. M. Wade, *J. Supercond.* **7**, 243 (1994).
- ³¹C. Panagopoulos, J. R. Cooper, and T. Xiang, *Phys. Rev. B* **57**, 13 422 (1998).
- ³²C. C. Homes, T. Timusk, D. A. Bonn, R. Liang, and W. N. Hardy, *Physica C* **254**, 265 (1995).